Causal influences of brain metabolic activity reveal interregional progressions in normal aging

Xin Di [1, 2], Marie Wölfer [1, 3, 4], Mario Amend [5], Hans Wehrl[5], Tudor M. Ionescu [5], Bernd J. Pichler [5], Bharat B. Biswal [1, 2, *], the Alzheimer's Disease Neuroimaging Initiative [#]

1. Department of Biomedical Engineering, New Jersey Institute of Technology, Newark, NJ, 07029, USA
2. School of Life Sciences and Technology, University of Electronic Science and Technology of China, Chengdu, China
3. Clinical Affective Neuroimaging Laboratory (CANLAB), Otto-von-Guericke-University Magdeburg, Magdeburg, Germany
4. Department for Behavioral Neurology, Leibniz Institute for Neurobiology, Magdeburg, Germany
5. Werner Siemens Imaging Center, Department of Preclinical Imaging and Radiopharmacy, Eberhard Karls University Tuebingen, Germany

* Corresponding author:
Bharat B. Biswal, PhD
607 Fenster Hall, University Height
Newark, NJ, 07102, USA
bbiswal@yahoo.com

Data used in preparation of this article were obtained from the Alzheimer's Disease Neuroimaging Initiative (ADNI) database (adni.loni.usc.edu). As such, the investigators within the ADNI contributed to the design and implementation of ADNI and/or provided data but did not participate in analysis or writing of this report. A complete listing of ADNI investigators can be found at: http://adni.loni.usc.edu/wp-content/uploads/how_to_apply/ADNI_Acknowledgement_List.pdf

Funding acknowledgements

This study was funded by (US) National Institute of Health grants: R01AT009829 and R01DA038895.

Running headline: Causal brain metabolic connectivity in aging

Abstract

During healthy brain aging, different brain regions show anatomical or functional declines or compensatory increases at different rates. However, few studies have explored the interregional causal influences during the aging process. We proposed a causality analysis framework combining high dimensionality independent component analysis (ICA), Granger causality, and LASSO (least absolute shrinkage and selection operator) regression on longitudinal brain metabolic activity data measured by Fludeoxyglucose positron emission tomography (FDG-PET). We analyzed FDG-PET images from healthy elderly subjects, who were scanned at least five sessions with an averaged intersession interval of about one year. The longitudinal data were concatenated across subjects to form a time series, and the first order autoregressive model was used to measure interregional causality among the independent sources of metabolic activity identified using ICA. Several independent sources with reduced metabolic activity in aging, including the anterior temporal lobe, orbital frontal cortex, anterior insula, and inferior parietal lobule, demonstrated causal influences over many other widespread brain regions, where themselves showed smaller age related declines. The current data demonstrated interregional progressions of aging on metabolic activity at the scale of a year, and demonstrated key brain regions in the aging process that have strong influences over other regions.

Keyword: aging, anterior temporal lobe, Granger causality, LASSO regression, metabolic connectivity.

1. Introduction

The human brain undergoes development and aging across the entire life-span. Neuroimaging studies have demonstrated that different brain regions develop and age in different rates. Although the global gray matter volume decreases linearly during aging, some regions such as the bilateral insula, superior parietal gyri, central sulci, and cingulate sulci show accelerated volumetric declines as measured by voxel-based morphometry [1]. Cortical thickness analysis has shown more widespread cortical thinning patterns during aging [2]. In contrast, results from functional MRI studies (fMRI) are more complex with some brain regions show increased activation in certain tasks rather than declined activation accompanied with anatomical declines [3,4]. In addition, the functional alterations in aging may depend on the task domains and behavioral outcomes [3], making it difficult to conclude a region to be functionally increased or decreased in aging. A complementary approach is to study brain activity during states without specific behavioral involvement, i.e. resting-state. Studies have been performed earlier using positron emission tomography (PET) imaging [5,6], and later using resting-state fMRI [7]. Using a large sample of over 1,000 subjects, Biswal and colleagues have showed reduced resting-state activity mainly in the default model network and increased activity in the visual, motor, and subcortical regions [7].

Functionally related brain regions typically show similar co-development [8] or co-decline, therefore yielding cross-subject interregional covariance patterns. This has been shown as early as 1980s using regional cerebral blood flow data [9] and on regional metabolic activity data [10,11] measured using PET. Later, more sophisticated methods, such as independent component analysis (ICA) and graph theory based analysis, have been applied to PET data to study the brain metabolic covariance networks [12,13]. Correlated metabolic activity or blood flow was typically found between left/right homotopic regions, and between some within hemisphere regions that are known to have functional relationships, e.g. language related regions in the left hemisphere. However, different connectivity patterns have been found between this metabolic covariance connectivity and the resting-state connectivity that has been typically observed

using fMRI data [12,13]. The inter-subject covariance patterns have also been shown using other imaging modalities, such as brain volumes [14–16], cortical thickness [17], and different resting-state fMRI indices [18,19].

Given the different rates of declines or relative reservations of different brain regions in aging, and large scale brain networks work in synchrony both during task execution and in resting-state [20,21], it is likely that the regions that are working together may affect each other during the aging process. Specifically, a region that declines faster may influence other functionally related regions by everyday functional interactions therefore would cause the other region to decline or show a compensatory increase. It is therefore critical to study the causal interregional influences between regions rather than the simple covariance, especially at the time scale of months to years when brain aging is occurring. Granger causality [22] may be a suitable method for this purpose, which examines the prediction of brain measures in one region over another brain region. Specifically, by using Granger causality we could examine whether the brain activity in a brain region at time points of months or years earlier can predict the activity of another brain region at the current time point. Granger causality at the similar time scales has been studied on brain morphological progressions in epilepsy [23] and schizophrenia [24] based on anatomical MRI data. However, both of these studies are cross-sectional. Large-scale multi-site longitudinal open access dataset, such as Alzheimer's Disease Neuroimaging Initiative (ADNI), has made it possible to examine causal influences during aging in a within-subject manner. Extending our previous work on metabolic covariance network using Fludeoxyglucose (FDG) PET images [12,13], we were able to examine the interregional causal influences of metabolic activity during aging.

The aim of the current study is to explore the causal interregional influences of metabolic activity during normal aging at the time scale of months to years. We leveraged the longitudinal FDG-PET data from the ADNI dataset, where there were at least five sessions of FDG-PET scans for each subject at a time step of approximately one year. First, we examined age effects of metabolic activity to identify regions with accelerated declines, with no apparent age effects, and with relative increases. Second, we performed whole brain Granger causality analysis to identify causal influences, where the metabolic

activity in a region in a certain time point can be predicted by the metabolic activity in another region at the previous time point. We predict that the regions that show accelerated declines during aging will cause other regions to decline, thus showing interregional progressions of age effects.

2. Materials and methods

2.1 ADNI data

Data used in the preparation of this article were obtained from the Alzheimer's Disease Neuroimaging Initiative (ADNI) database (adni.loni.usc.edu). The ADNI was launched in 2003 as a public-private partnership, led by Principal Investigator Michael W. Weiner, MD. The primary goal of ADNI has been to test whether serial magnetic resonance imaging (MRI), positron emission tomography (PET), other biological markers, and clinical and neuropsychological assessment can be combined to measure the progression of mild cognitive impairment (MCI) and early Alzheimer's disease (AD). For up-to-date information, see www.adni-info.org.

We manually selected longitudinal FDG-PET images from the ADNI database. Specifically, we chose the healthy subjects who had at least five sessions of FDG-PET images available. As a result, 72 subjects (25 females) were included in the current analysis with a total of 432 PET scan sessions. The numbers of available sessions ranged from 5 to 9 (Figure 1A). The average age at the first session was 75.8 years (62 to 86 years). For each session, we calculated a mean image or adopted the only image to represent the session. The main analysis focused on the changes and causal influences over the time scale of sessions. The intersession interval with a subject varied from 3 months to up to 8 years for a few rare cases (Figure 1B). The mean and median of the intersession intervals were 1.02 and 0.98 years, respectively.

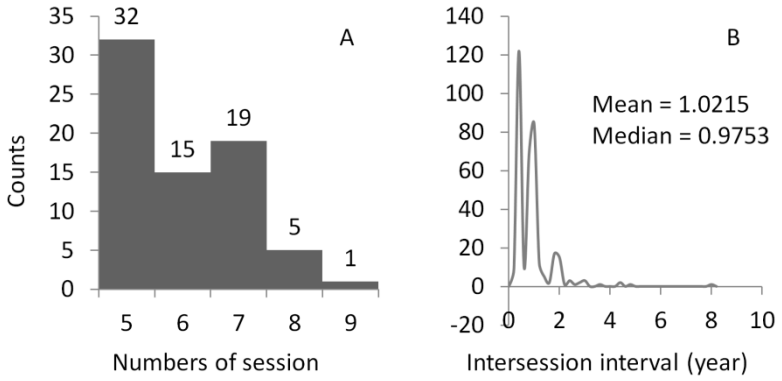

Figure 1 Histograms of the numbers of sessions for each subject (A) and the intersession intervals for all the sessions and subjects (B).

The FDG-PET images were acquired from multiple sites with different PET imaging protocols. However, the imaging parameters were mostly similar across different sessions within a subject. Since the current analyses were all within-subject, the impacts of different imaging parameters from different sites can be effectively minimized. All the images and subjects included in the current analysis are listed in the supplementary materials.

2.2. PET data preprocessing

The PET data were preprocessed using SPM12 (https://www.fil.ion.ucl.ac.uk/spm/) under MATLAB R2017b. For each subject, if there were more than one PET image in a session, all the PET images in the session were realigned to the first image and one mean image of a session was calculated. The mean images (or the only image) across all the sessions of a subject were then realigned to the image obtained in the first session. The cross-session mean image was normalized directly to the PET template in the standard MNI space (Montreal Neurological Institute), and then all the images were normalized to MNI space using the same set of parameters. We chose the direct normalization approach rather than using an anatomical MRI as a mediator, because the spatial resolutions of the PET images were adequate and the direct normalization has its own advantage compared with the anatomical MRI mediated method [25]. The

images were then spatially smoothed using a Gaussian kernel with 8 mm FWHM (full width at half maximum). Lastly, each image was divided by its mean signal within an intracranial volume mask.

2.3. Independent component analysis

We first performed spatial ICA to parcellate the whole brain metabolic maps into independent sources or independent components (ICs), which were representative of local metabolic variations [26,27]. We extracted a relatively high number of ICs, so that the resulting ICs could represent more local variations than large scale networks [28]. The ICA was performed using Group ICA of fMRI Toolbox (GIFT) (http://mialab.mrn.org/software/gift) [29]. The preprocessed FDG-PET images from different sessions and subjects were concatenated into a single time series, and fed into the ICA analysis. Eighty one components were recommended by the minimum description length (MDL) algorithm implemented in GIFT. After IC extraction of the 81 components, the ICs were visually inspected and categorized into eight networks (Figure 2) and noise components. There were in total 61 ICs included in the following analysis after excluding the 20 noise components. For each IC, the associated time series were obtained to represent metabolic activity of this source in different subjects and sessions.

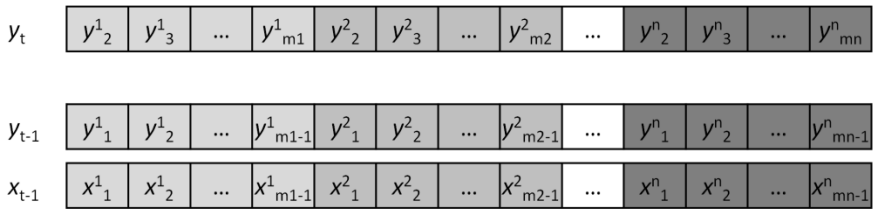

Figure 2 Independent components (ICs) representing independent sources of metabolic variations sorted into eight functional domains. The eight functional domains were used for illustration purpose only. Each IC map was threshoded at z > 2.3. The numbers in the brackets represent the number of ICs in each domain.

2.4. Regional age effects

For each subject, a general linear model (GLM) was built to examine the linear aging effect. The GLM included two regressors, a constant term and a linear age effect. The GLM analysis was performed on each IC, and the β values of the age effect were obtained. Group level analysis was then performed on each IC using a one sample t test model to examine the group averaged effect of age. A FDR (false discovery rate) corrected $p < 0.05$ was used to identify ICs that had significant age effects after correcting for all the 61 comparisons. Thereafter, the ICs were sorted into three groups, ICs with significant (relative) increased metabolic activity, ICs with no significant changes, and ICs with significant decreased metabolic activity in aging.

2.5. Interregional causality analysis

We adopted Granger causality like method to examine the interregional causal influence of metabolic activity. Specifically, we treated the longitudinal FDG-PET data as time series, and used autoregressive model to predict the value of time point t in a region *y* by the previous time points of another region *x*, when controlling for its own previous time points of *y*. In the current data, the time step is approximately one year. To account for the variability of intersession interval, the intervals between time points t and t – 1 were added as a covariate or regressed out in the analysis (see below for details). Another consideration is the order of the model, i.e. how many previous time points are used to predict the current time point. In this study, we used only the first order model to measure the causal influence of only one previous time point, which represents a time step of about one year. The limited number of time points in a subject prevents us to use higher order models. The advantage of using only the first order model is that the sign information of the beta estimate enables us to differentiate positive and negative prediction effects. The model can be expressed in the following form:

$$y_t = \beta_0 + \beta_1 \cdot y_{t-1} + \beta_2 \cdot x_{t-1} + \varepsilon$$

where *y* represents the predicted time series in one brain region, and *x* represents the predicting time series of another brain region. y_{t-1} represent the time series of y_t which moved one time point ahead, thus

representing a autoregression model of time series y_t. The effect of interest is the predicting value of x_{t-1}, which is β_2.

We concatenated the time series across all the subjects to form a long time series for analysis (Figure 3). Therefore, the model is considered fixed effect model. The first to m_i time series of a subject were first z transformed to minimize inter-subject variation, where m_i represents the total number of time points in a subject i. For each subject, we included the time points 2 to m of a region as the predicted variable y_t. The autoregressive variable y_{t-1} of the same region included the time points 1 to m - 1. The predicting variable x_{t-1} was the time points 1 to m – 1 from another region x. After concatenation, there were in total 360 data points in the time series.

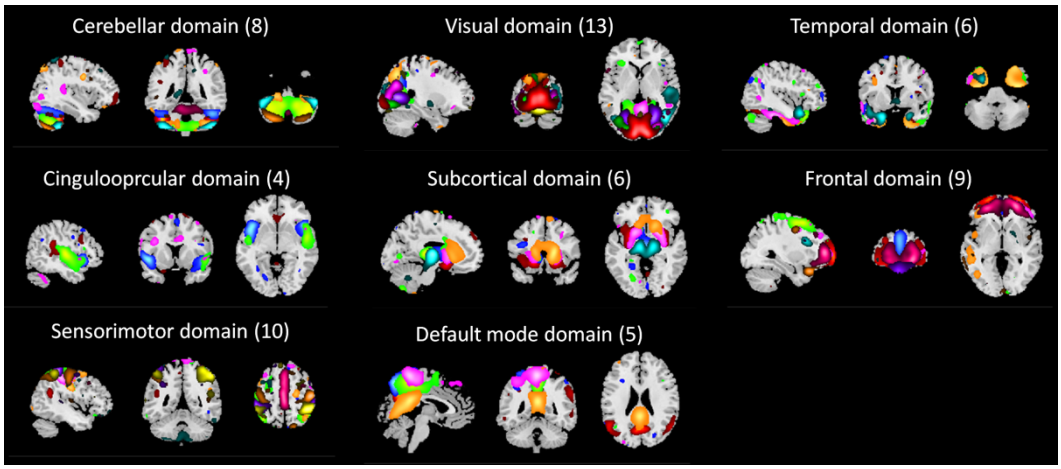

Figure 3 Illustration of the construction of the variables used in the causality analysis. X represents the predicting region, and y represents the predicted region. The superscript represents different subjects, with a total number of n. The subscript represents the scan session in a subject, with a total number of mi for a subject i.

The model could be applied to each pair of the ICs from the 61 ICs. The intersession interval between time t and time $t - 1$ were included in the model as a covariate. We first performed such analysis on each pair of ICs to obtain the predicting effect (β_2) and corresponding p values, which formed a 61 x

61 matrix of causal effects. FDR correction at $p < 0.05$ was used to correct for multiple comparisons of the in total 3,660 (61 x 60) effects, where autoregressive effects along the diagonal were not tested.

This pair-wise approach may identify influences from different regions with shared variance although maybe only one region has direct influence with the tested region. To overcome this, when predicting a region x^i_t, one can add all the other ICs to identify which region can predict x^i_t. The model is then as following for a predicted region x^i:

$$x_t^i = \beta_0 + \beta_1 \cdot x_{t-1}^1 + \beta_2 \cdot x_{t-1}^2 + \beta_3 \cdot x_{t-1}^3 + \ldots + \beta_p \cdot x_{t-1}^p + \varepsilon$$

Since all the ICs were included in the model, there was no need to differentiate the variables of *x* and *y*. Therefore, we use *x* to denote all the time series variables. The superscripts of *x* now represent different ICs, where p represents the total number of the IC. Before entering in to the model, a time series representing the intersession interval between time point t and t – 1 were regressed out from all the x_{t-1} time series to account for the intersession interval variability. Estimating the multivariate model may be challenging, especially when some of the IC time series may be highly correlated. It can be assumed that only a small number of ICs may influence the predicted IC. In this scenario, one can use regularization method to estimate the sparse influence effects, such as using LASSO (least absolute shrinkage and selection operator) [30,31]. The motivation of choosing LASSO over other regularization methods is that the LASSO regularization can force some parameters in the model to be zero thus resulting in only a small number of non-zero parameters. This is important in the current context, because the aim is to identify a small number of interregional influences. Since this model examines the prediction of the time series of one IC by the time series of all the other ICs, the analysis only needed to be performed for 61 times (compared with 61 x 60 times in the pair-wise analysis) to cover all the ICs.

The LASSO regression was performed using the lasso function implemented in MATLAB. To determine an optimal regularization factor λ, we used a set of λ from 0 (no regularization) to 0.5 with a step of 0.001. The identified non-zero influences dropped dramatically as the increase of λ. We identify

the λ where the number of non-zero influences were the closest to the number of significant effects when using FDR correction in pair-wise analysis, and reported all non-zero influencing effects.

The resulting 61 x 61 influencing matrix can be treated as a directed network graph, where the ICs represent the nodes and the causal influences represent directed edges of the graph. We calculated in-degree and out-degree of the 61 nodes to characterize the importance of an IC in the whole brain influencing graph. To ensure that the degree calculation was not affected by arbitrary defined threshold, we also explored the graphs from other λ values to verify the identified hub regions are still present. To visualize the network topology, we identified the giant component where all the nodes in the component were somehow connected (without considering the direction of the influences). The giant components were visualized using the force layout.

3. Results

3.1. The age effect on regional metabolic activity

We first examined the age effects on the regional metabolic activity for the 61 ICs. Statistical significant ICs at $p < 0.05$ after FDR correction are shown in Figure 4. Eighteen ICs showed significant reduced metabolic activity, including several ICs covering visual regions, anterior lateral or medial temporal regions, bilateral insula, prefrontal regions, cingulate cortex from the anterior portion to the posterior portion, and the cerebellum. In contrast, 6 ICs showed increased metabolic activity. It should be noted that due to the nature of PET imaging, the global signal for each PET image has to be normalized. Therefore, it is difficult to say whether the positive age effect represents increased metabolic activity, or a relative increase with reference to the global effect. These ICs with relative increased metabolic activity during aging included the inferior portion of the cerebellum, subcortical regions covering the basal ganglia, insula, amygdala, and thalamus, and sensorimotor regions.

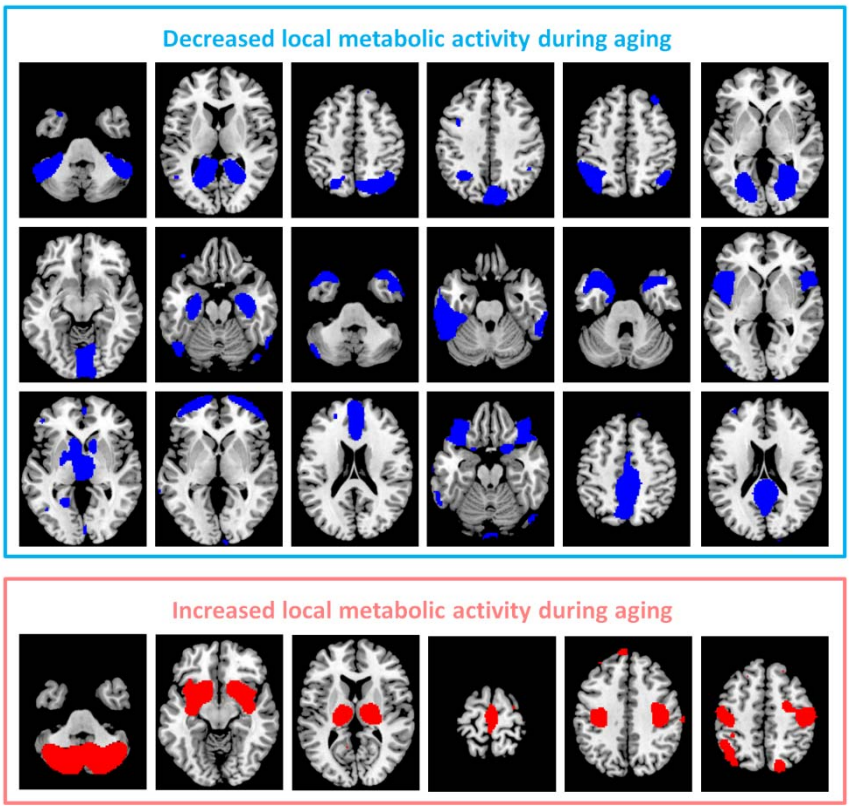

Figure 4 The independent components (ICs) that showed statistically significant decreased (blue) and increased (red) metabolic activity during aging after controlling for global effect at $p < 0.05$ with false discovery rate (FDR) correction.

3.2. Interregional causal influences of metabolic activity

We first applied pairwise autoregressive model to obtain a 61 x 61 matrix of the interregional causal influences of metabolic activity between each pair of the 61 ICs (Figure 5A). When using a statistical threshold of $p < 0.05$ of FDR correction, 15 positive and 13 negative causal influences were identified (Figure 5B). We next performed LASSO regression with x_t of an IC as the predicted variable and x_{t-1} of all the ICs as the predicting variables using a range of λ. We identified the λ value where the number of non-zero effects was the closest to the number of significant effects in the pairwise analysis. The resulting influencing effects at $\lambda = 0.16$ (Figure 5C) look in general similar to the significant effects

identified by the pairwise analysis, although some subtle differences can be noted. There were 16 positive and 12 negative causal influences identified using the LASSO regression method.

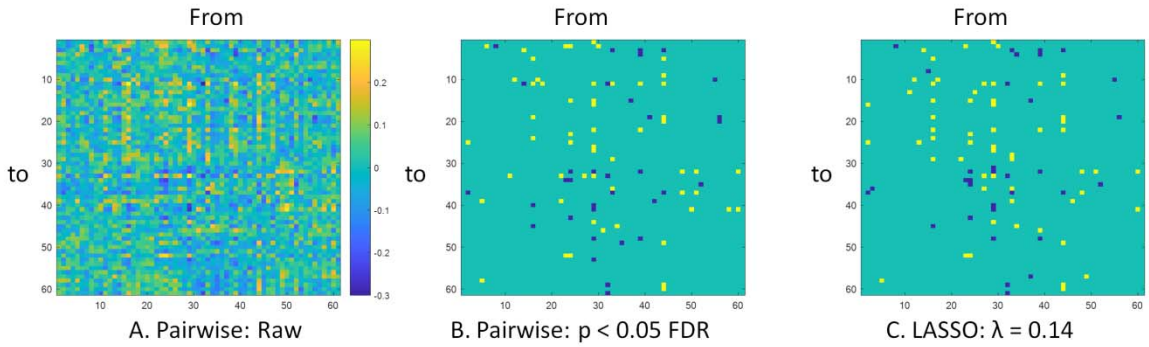

Figure 5 A, Pairwise matrix of interregional causal influence of metabolic activity. The columns represent influencing ICs, while the rows represent influenced ICs. B, Ternary matrix of significant positive or negative interregional causal influences thresholded at $p < 0.05$ after false discovery rate (FDR) correction. C, Ternary matrix of positive or negative interregional causal influences identified at $\lambda = 0.16$ using LASSO (least absolute shrinkage and selection operator) regression.

Among the 28 causal influences from the LASSO regression analysis, the first giant component was comprised of 25 causal influences involving 24 ICs (Figure 6). The IC maps were color coded based on the age effects on metabolic activity to illustrate the relationships between regional metabolic activity changes and the signs of causal influences. It can be seen that the influences between two decreased regions or two increased regions were in general positive, but the influences between one increased region and one decreased region were in general negative. For example, the bilateral anterior temporal IC (# 14 in Figure 6) positively influenced the medial parietal IC (# 13), but negatively influenced the bilateral basal ganglia IC (# 15). It is consistent with the direction of the progression of age effects. Of course, there were also ICs that without apparent age effects, where the sign of causal influences with other regions did not show clear pattern.

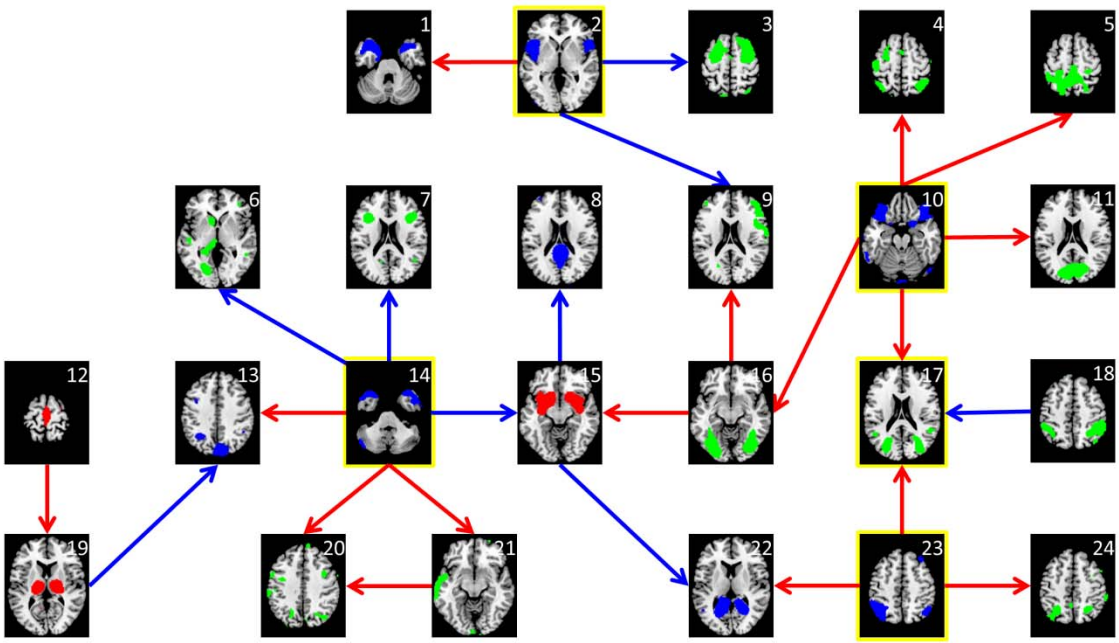

Figure 6 The first giant component of interregional causal influences network at λ of 0.16. The colors of the independent component maps represent increased (red), decreased (blue), and non-significant effects (green) of metabolic activity with age. The colors of the arrows represent positive (red) and negative (blue) interregional influences, respectively. The maps highlighted with yellow frames represent hub regions in the network.

Several ICs showed more influencing effects to other ICs. Figure 6 highlights the four influencing hubs that have greater than or equal to three out-degrees, including the bilateral anterior temporal IC (# 14), bilateral orbitofrontal IC (# 10), bilateral insula IC (# 2), and bilateral inferior parietal IC (# 23). In addition, the bilateral dorsal occipital IC (# 17) was influenced by three ICs. To better illustrate the topology of the causal influencing network and to highlight the regions that were more influencing or influenced to other regions, we plotted the first giant components of the interregional influencing network using force layout at λ = 0.16, and also at more liberal thresholds of λ = 0.14 and λ = 0.12 (Figure 7). The node sizes represent the out-degree or in-degree of a node in the network. It can be seen that the out-degree hubs were in general the regions with decreased metabolic activity (blue nodes).

And the four influencing hubs identified at λ = 0.16 were still the influencing hubs at lower λ values. While in terms of in-degree, there were no clear regions that had exceptionally high in-degree with other nodes. The node with high in-degree had no apparent age effects (green nodes) or had increased metabolic activity with age (red nodes). The influenced hub identified at λ = 0.16 no longer had the highest in-degree at lower λ values, and had very similar in-degrees with many other nodes.

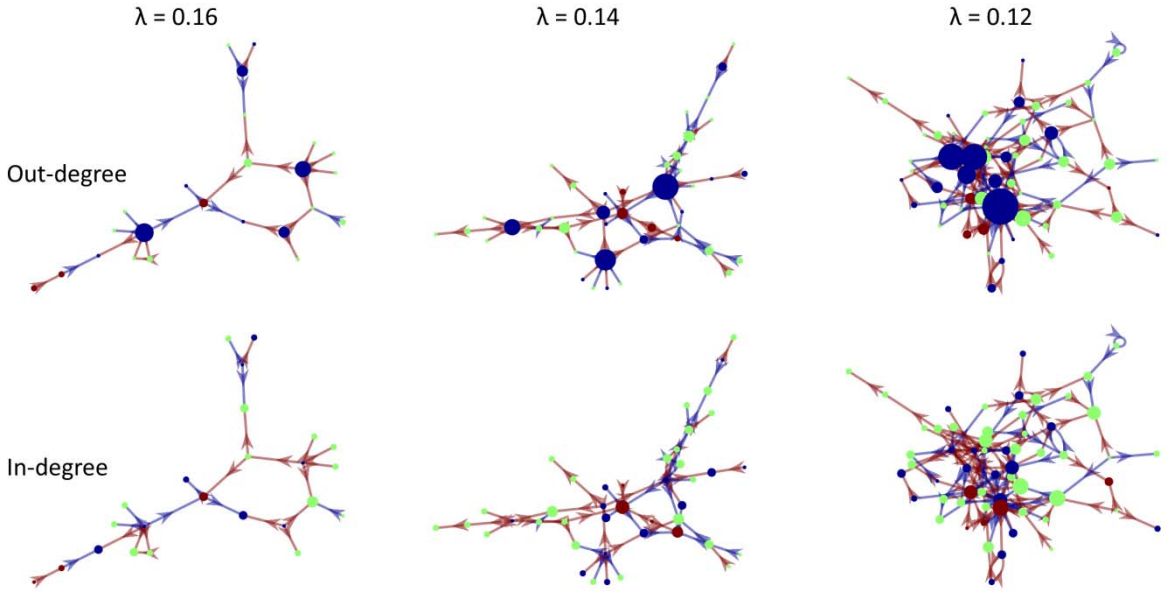

Figure 7 The giant component of the causal interregional influence network of metabolic activity at different λ levels with the sizes of the nodes reflecting out-degree (top row) and in-degree (bottom row). Red and blue arrows indicate positive and negative influences identified using LASSO regression. Blue, green, and red regions indicate positive, none, and negative age effects on regional metabolic activity.

4. Discussion

By applying autoregressive model on longitudinal FDG-PET data, the current study demonstrated causal interregional influences of metabolic activity during normal aging. Several ICs with significant reduced metabolic activity in aging, including the anterior temporal lobe, orbital frontal cortex, anterior insula, and inferior parietal lobule, causally influenced many other ICs. In contrast, the influenced ICs were more

widespread and with less local aging effects or even with relatively increased metabolic activity. To the best of our knowledge, this is the first study to demonstrate longitudinal interregional causal influences of brain activity during aging at the time scale of a year.

Consistent with our prediction of interregional progressions of age effects, the influencing ICs usually had decreased metabolic activity. On the other hand, the influenced regions were not restricted to the regions with reduced metabolic activity in aging. Indeed, the ICs that had relatively greater in-degree values than other ICs were usually without apparent age effects, or even with relatively increased metabolic activity, e.g. the basal ganglia and thalamus. Therefore, the causal interregional influences in general reflected the spread of age effects from the brain regions that had already declined to the regions that are declining, relatively reserved, or even show a compensatory increased metabolic activity. We note that the absence of regional age effects should be interpreted with caution, because the removal of global effects during calculation of regional age effects could have removed significant age effects that were similar to the global effects.

The interpretation of the causal influences need to consider both the sign of the causal influences and the regional age effects. A positive influence indicates that the metabolic activity in region A at the current time point positively predicts the metabolic activity in region B at the next time point. While a negative influence indicates a negative prediction. If the two regions are both decreasing during aging, then a positive influence may indicate a spread of metabolic activity decline between the two regions during aging. On the other hand, if region A showed decreased but region B showed non-significant age effect or relatively increased metabolic activity, and there was a negative influence between A and B, then it may indicate a compensation of region B that is resulted from the declined function of region A. A close look at the patterns of the directions of the local and interregional effects, we found that most of the effects observed were consistent with this progression or compensation interpretation. No negative causal influences were found between two regions that both showed negative effects. The regions that did not

show statistically significant age effects were mostly influenced by other regions. The sign of the causal influences could be either positive or negative.

The current analysis identified several hubs that influenced other brain regions, including the anterior temporal lobe, orbital frontal cortex, anterior insula, and inferior parietal lobule. These regions all showed age related decline of metabolic activity, and are mostly involved in higher functions. In order to better characterize the functions of these hub ICs, we submit the IC maps into NeuroVault (https://neurovault.org), and decoded the functions of these maps using large-scale meta-analytic data from Neurosynth (http://neurosynth.org/) [32]. The first five functional terms that are associated with the anterior temporal IC are all about language and semantic processing (See Supplementary Table S1). Studies also showed that electrical stimulation of the anterior temporal lobe can improve proper name recalls in aging [33], and bilingualism can protect the integrity of anterior temporal lobe in aging [34]. The functional words related to the orbital frontal IC were mainly about emotional processing. And in elderly population, smaller orbital frontal volumes are shown to be associated with depression [35,36]. The anterior insula IC is a major part of the salience network [37] and very functionally heterogeneous [38]. Likewise, the decoded functional keywords ranged from emotion, music, to language processes. Lastly, the functional words related to the inferior parietal IC are mainly about memory retrieval. And there is also evidence of neuroprotective effects of bilingualism on the inferior parietal lobule in elderly population [39].

If there is long term causal influence between two brain regions during aging, it is likely due to everyday functional interactions between the regions. Therefore, we would expect the causal influences to take place between functionally related brain regions. Indeed, the influencing ICs are all connected to major white matter tracts, which could support their functional influences over the other brain regions during aging. For example, the anterior temporal lobe is connected to the cingulum, inferior longitudinal fasciculus, and uncinate fasciculus, the orbital frontal cortex is connected to the uncinate fasciculus and inferior fronto-occipital fasciculus, the anterior insula is connected to the uncinate fasciculus, and the inferior parietal lobule is connected to the arcuate fasciculus [40].

A limitation of the current analysis is the potential confounding effect due to partial volume. However, the following reasons make the partial volume confounding less problematic. First, the current analysis adopted within subject comparison, which has already minimized the partial volume effects due to inter subject anatomical variability. Second, we applied ICA analysis to identify independent sources of metabolic variability. Some components that were likely due to enlargement of ventricle may be spatially overlapped with the included ICs, have been already removed. For example, there was an IC largely located in ventricle area but with substantial overlaps with the ICs of the thalamus and basal ganglia (IC 79 in supplementary Figure S1). The IC had the second strongest negative age effect among all the ICs. The included ICs that had spatial overlap with this IC showed no age effects or even positive age effects, suggesting that the partial volume effects associated with enlarged ventricle have been minimized in these ICs. Third, even though the observed causal influences may still somehow contributed by the residual partial volume effects, the causal influences of volumetric reductions may still be important findings in the aging process. The MRI images are available in the ADNI dataset, but are not always acquired at the same time point as the PET images, making the implementation of MRI images in the model difficult. Future studies should certainly consider taking into account of anatomical information in the analysis. But indeed, it may be more important to study the interaction or causal influences between different modalities in aging, because the aging brain undergo dynamic compensation process [41]. According to the compensation model, the reduction of gray matter will lead to elevated functional responses, which then give rise to less affected behavioral performances [41]. A direct examination of causal influences among local gray matter structures, functions, and behavioral performances may provide more insight to the dynamic of compensation process in aging.

One strength of the current analysis approach is that we adopted multivariate methods and LASSO to include all the ICs in the predicting models, which in theory can prevent identifying ICs that have indirect predicting effects to the target [31,42]. On the other hand, there are also several simplifications of the Granger causality analysis, such as the inclusion of only the first order model and the assumption of

equal time steps. Since the current study is the first to explore the causality in the aging process, the time lag of the aging progression is still largely unknown and bear further studies. But practically due to the limited availability of longitudinal data, this question is difficult to solve at the current stage. Regarding the variable time steps of the time series, we added the intersession interval as a covariate to minimize the effects, which is similar to a previous work [24]. More sophisticated model, such as generative model and differential equation based method [43,44], may be used in the future to better characterize the causal effects.

5. Conclusion

By applying Granger causality analysis on longitudinal FDG-PET images of elderly healthy participants at a time step of one year, the current analysis revealed interregional causal influences during aging. Several regions with a reduction in local metabolic activity during aging, including the bilateral anterior temporal lobe, orbitofrontal cortex, and anterior insula, showed causal influences with other regions, supporting an interregional progression of age effects in the brain. The current analysis and results could add new insights to the neurocognitive aging literature about interregional interactions during the aging process.

Acknowledgements

Data collection and sharing for this project was funded by the Alzheimer's Disease Neuroimaging Initiative (ADNI) (National Institutes of Health Grant U01 AG024904) and DOD ADNI (Department of Defense award number W81XWH-12-2-0012). ADNI is funded by the National Institute on Aging, the National Institute of Biomedical Imaging and Bioengineering, and through generous contributions from the following: AbbVie, Alzheimer’s Association; Alzheimer’s Drug Discovery Foundation; Araclon Biotech; BioClinica, Inc.; Biogen; Bristol-Myers Squibb Company; CereSpir, Inc.; Cogstate; Eisai Inc.; Elan Pharmaceuticals, Inc.; Eli Lilly and Company; EuroImmun; F. Hoffmann-La Roche Ltd and its affiliated company Genentech, Inc.; Fujirebio; GE Healthcare; IXICO Ltd.; Janssen Alzheimer

Immunotherapy Research & Development, LLC.; Johnson & Johnson Pharmaceutical Research & Development LLC.; Lumosity; Lundbeck; Merck & Co., Inc.; Meso Scale Diagnostics, LLC.; NeuroRx Research; Neurotrack Technologies; Novartis Pharmaceuticals Corporation; Pfizer Inc.; Piramal Imaging; Servier; Takeda Pharmaceutical Company; and Transition Therapeutics. The Canadian Institutes of Health Research is providing funds to support ADNI clinical sites in Canada. Private sector contributions are facilitated by the Foundation for the National Institutes of Health (www.fnih.org). The grantee organization is the Northern California Institute for Research and Education, and the study is coordinated by the Alzheimer's Therapeutic Research Institute at the University of Southern California. ADNI data are disseminated by the Laboratory for Neuro Imaging at the University of Southern California.

Author contributions:

X.D. conceived the idea, developed and performed the data analysis. All authors discussed the results, and contributed to the final manuscript.

Conflict of interest statement:

The authors declare that there is no conflict of interest regarding the publication of this article.

Supplemental materials:

Supplemental materials include one word file containing one supplementary Table S1 and one supplementary Figure S1, and one csv file listing all the PET image files downloaded from the ADNI database.

Reference:

1. Good CD, Johnsrude IS, Ashburner J, et al. A voxel-based morphometric study of ageing in 465 normal adult human brains. *Neuroimage* 2001; 14: 21–36.

2. Salat DH, Buckner RL, Snyder AZ, et al. Thinning of the cerebral cortex in aging. *Cereb Cortex* 2004; 14: 721–730.

3. Spreng RN, Wojtowicz M, Grady CL. Reliable differences in brain activity between young and old adults: A quantitative meta-analysis across multiple cognitive domains. *Neurosci Biobehav Rev* 2010; 34: 1178–1194.

4. Di X, Rypma B, Biswal BB. Correspondence of executive function related functional and anatomical alterations in aging brain. *Prog Neuropsychopharmacol Biol Psychiatry* 2014; 48: 41–50.

5. Zuendorf G, Kerrouche N, Herholz K, et al. Efficient principal component analysis for multivariate 3D voxel-based mapping of brain functional imaging data sets as applied to FDG-PET and normal aging. *Hum Brain Mapp* 2003; 18: 13–21.

6. Martin AJ, Friston KJ, Colebatch JG, et al. Decreases in Regional Cerebral Blood Flow with Normal Aging. *J Cereb Blood Flow Metab* 1991; 11: 684–689.

7. Biswal BB, Mennes M, Zuo X-N, et al. Toward discovery science of human brain function. *Proc Natl Acad Sci U S A* 2010; 107: 4734–9.

8. Alexander-Bloch A, Raznahan A, Bullmore E, et al. The convergence of maturational change and structural covariance in human cortical networks. *J Neurosci* 2013; 33: 2889–99.

9. Prohovnik I, Håkansson K, Risberg J. Observations on the functional significance of regional cerebral blood flow in ‘resting’ normal subjects. *Neuropsychologia* 1980; 18: 203–17.

10. Metter EJ, Riege WH, Kuhl DE, et al. Cerebral Metabolic Relationships for Selected Brain Regions in Healthy Adults. *J Cereb Blood Flow Metab* 1984; 4: 1–7.

11. Horwitz B, Duara R, Rapoport SI. Intercorrelations of Glucose Metabolic Rates Between Brain Regions: Application to Healthy Males in a State of Reduced Sensory Input. *J Cereb Blood Flow Metab* 1984; 4: 484–499.

12. Di X, Biswal BB, Alzheimer’s Disease Neuroimaging Initiative. Metabolic brain covariant

networks as revealed by FDG-PET with reference to resting-state fMRI networks. *Brain Connect* 2012; 2: 275–83.

13. Di X, Gohel S, Thielcke A, et al. Do all roads lead to Rome? A comparison of brain networks derived from inter-subject volumetric and metabolic covariance and moment-to-moment hemodynamic correlations in old individuals. *Brain Struct Funct* 2017; 222: 3833–3845.

14. Mechelli A, Friston KJ, Frackowiak RS, et al. Structural covariance in the human cortex. *J Neurosci* 2005; 25: 8303–10.

15. Douaud G, Groves AR, Tamnes CK, et al. A common brain network links development, aging, and vulnerability to disease. *Proc Natl Acad Sci* 2014; 111: 17648–17653.

16. Di X, Biswal BB. Similarly Expanded Bilateral Temporal Lobe Volumes in Female and Male Children With Autism Spectrum Disorder. *Biol Psychiatry Cogn Neurosci Neuroimaging* 2016; 1: 178–185.

17. Lerch JP, Worsley K, Shaw WP, et al. Mapping anatomical correlations across cerebral cortex (MACACC) using cortical thickness from MRI. *Neuroimage* 2006; 31: 993–1003.

18. Taylor PA, Gohel S, Di X, et al. Functional covariance networks: obtaining resting-state networks from intersubject variability. *Brain Connect* 2012; 2: 203–17.

19. Zhang Z, Liao W, Zuo X-N, et al. Resting-state brain organization revealed by functional covariance networks. *PLoS One* 2011; 6: e28817.

20. Bullmore E, Sporns O. Complex brain networks: graph theoretical analysis of structural and functional systems. *Nat Rev Neurosci* 2009; 10: 186–98.

21. Bullmore E, Sporns O. The economy of brain network organization. *Nat Rev Neurosci* 2012; 13: 336–349.

22. Granger CWJ. Investigating Causal Relations by Econometric Models and Cross-spectral Methods. *Econometrica* 1969; 37: 424.

23. Zhang Z, Liao W, Xu Q, et al. Hippocampus-associated causal network of structural covariance

measuring structural damage progression in temporal lobe epilepsy. *Hum Brain Mapp* 2017; 38: 753–766.

24. Jiang Y, Luo C, Li X, et al. Progressive Reduction in Gray Matter in Patients with Schizophrenia Assessed with MR Imaging by Using Causal Network Analysis. *Radiology* 2018; 287: 633–642.

25. Calhoun VD, Wager TD, Krishnan A, et al. The impact of T1 versus EPI spatial normalization templates for fMRI data analyses. *Hum Brain Mapp* 2017; 38: 5331–5342.

26. Fu Z, Tu Y, Di X, et al. Transient increased thalamic-sensory connectivity and decreased whole-brain dynamism in autism. *Neuroimage*. Epub ahead of print June 2018. DOI: 10.1016/j.neuroimage.2018.06.003.

27. Fu Z, Tu Y, Di X, et al. Characterizing dynamic amplitude of low-frequency fluctuation and its relationship with dynamic functional connectivity: An application to schizophrenia. *Neuroimage* 2018; 180: 619–631.

28. Smith SM, Vidaurre D, Beckmann CF, et al. Functional connectomics from resting-state fMRI. *Trends Cogn Sci* 2013; 17: 666–682.

29. Calhoun VD, Adali T, Pearlson GD, et al. A method for making group inferences from functional MRI data using independent component analysis. *Hum Brain Mapp* 2001; 14: 140–51.

30. Tibshirani R. Regression Selection and Shrinkage via the Lasso. *Journal of the Royal Statistical Society B* 1996; 58: 267–288.

31. Tang W, Bressler SL, Sylvester CM, et al. Measuring Granger Causality between Cortical Regions from Voxelwise fMRI BOLD Signals with LASSO. *PLoS Comput Biol* 2012; 8: e1002513.

32. Rubin TN, Koyejo O, Gorgolewski KJ, et al. Decoding brain activity using a large-scale probabilistic functional-anatomical atlas of human cognition. *PLOS Comput Biol* 2017; 13: e1005649.

33. Ross LA, McCoy D, Coslett HB, et al. Improved Proper Name Recall in Aging after Electrical Stimulation of the Anterior Temporal Lobes. *Front Aging Neurosci*; 3. Epub ahead of print 2011.

DOI: 10.3389/fnagi.2011.00016.

34. Abutalebi J, Canini M, Della Rosa PA, et al. Bilingualism protects anterior temporal lobe integrity in aging. *Neurobiol Aging* 2014; 35: 2126–2133.

35. Lai T-J, Payne ME, Byrum CE, et al. Reduction of orbital frontal cortex volume in geriatric depression. *Biol Psychiatry* 2000; 48: 971–975.

36. Taylor WD, Steffens DC, McQuoid DR, et al. Smaller orbital frontal cortex volumes associated with functional disability in depressed elders. *Biol Psychiatry* 2003; 53: 144–149.

37. Seeley WW, Menon V, Schatzberg AF, et al. Dissociable intrinsic connectivity networks for salience processing and executive control. *J Neurosci* 2007; 27: 2349–56.

38. Seeley WW. Anterior insula degeneration in frontotemporal dementia. *Brain Struct Funct* 2010; 214: 465–475.

39. Abutalebi J, Canini M, Della Rosa PA, et al. The neuroprotective effects of bilingualism upon the inferior parietal lobule: A Structural Neuroimaging Study in Aging Chinese Bilinguals. *J Neurolinguistics* 2015; 33: 3–13.

40. Catani M, Thiebaut de Schotten M. A diffusion tensor imaging tractography atlas for virtual in vivo dissections. *Cortex* 2008; 44: 1105–32.

41. Gregory S, Long JD, Klöppel S, et al. Testing a longitudinal compensation model in premanifest Huntington's disease. *Brain*. Epub ahead of print 17 May 2018. DOI: 10.1093/brain/awy122.

42. Smith SM, Miller KL, Salimi-Khorshidi G, et al. Network modelling methods for FMRI. *Neuroimage* 2011; 54: 875–891.

43. Ziegler G, Ridgway GR, Blakemore S-J, et al. Multivariate dynamical modelling of structural change during development. *Neuroimage* 2017; 147: 746–762.

44. Ziegler G, Penny WD, Ridgway GR, et al. Estimating anatomical trajectories with Bayesian mixed-effects modeling. *Neuroimage* 2015; 121: 51–68.